TWIST BUCKLING AND THE FOLDABLE CYLINDER: AN EXERCISE IN ORIGAMI

Giles W. Hunt* Ichiro Ario **
*Centre for Nonlinear Mechanics, University of Bath, Bath BA2 7AY, UK
**Department Civil and Environmental Engineering, Hiroshima University, Higashi-Hiroshima, 739-8527, Japan

Summary When a tube of paper is twisted between two rigid plastic mandrels (see Fig.1), a mechanism familiar from the Japanese art of origami develops, involving bending but little stretching. But the initial buckling problem of a cylindrical shell under torsion (see Fig.2) involves bending and stretching energies in about equal parts. The talk will trace the consequent adjustment of the modeshape though first-order post-buckling, to the final folded pattern, as seen from the viewpoint of a triangulated truss formulation.

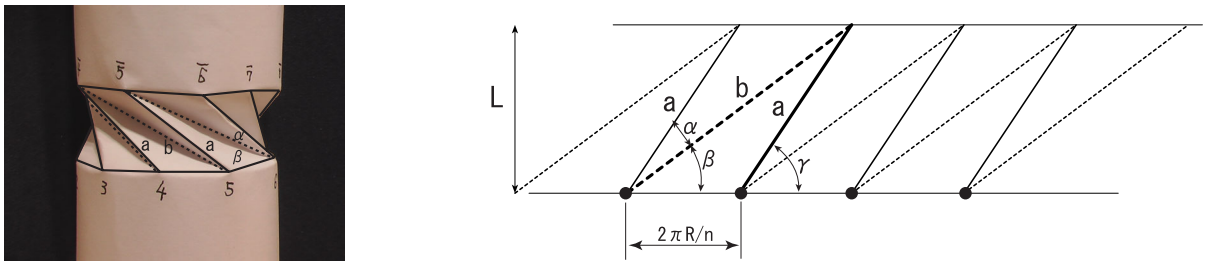

(a) Fold lines and angles of the folding mechanism (b) Truss Geometry

Figure 1. The foldable cylinder based on twist buckling of a paper roll. Large deflections involve work being done primarily against bending, with very little stretching energy included; such behaviour is of interest for example, in the field of deployable structures.

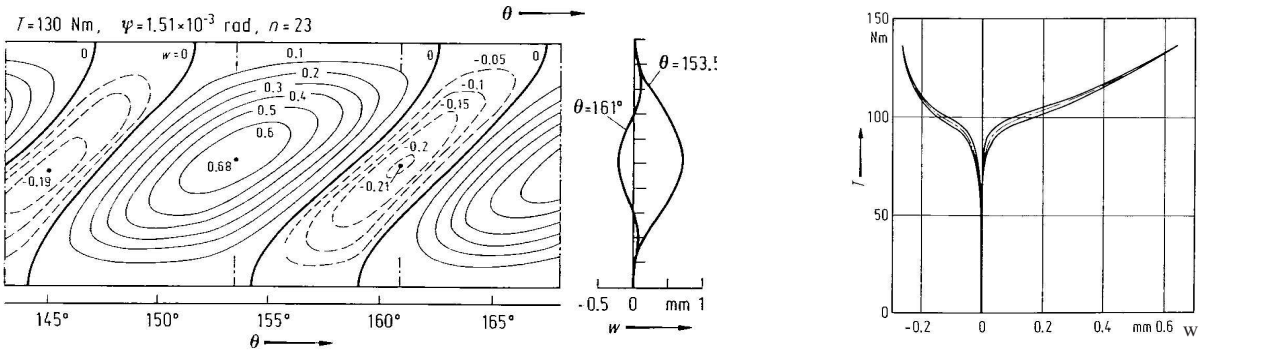

(a) Contour of deformation (b) Relationship between torque and $w(L/2, y)$

Figure 2. Yamaki's shortest cylindrical shell buckling in torsion [1]. Length L = 22.9 mm, Radius $R = 100$ mm, thickness t = 0.247 mm, Young's modulus $E = 5.55$ GPa, Poisson's ratio $\nu = 0.3$.

FORMULATION AND LINEAR EIGENVALUE ANALYSIS

Critical buckling and first-order post buckling analyses are based on the total potential function

$$\begin{aligned} V &= \frac{Et^3}{24(1-\nu^2)} \int_0^L\!\!\int_0^{2\pi R} \left\{ \left(\nabla^2 w\right)^2 + 2(1-\nu)\left[(w_{xy})^2 - w_{xx}w_{yy}\right] \right\} \mathrm{d}y\mathrm{d}x \\ &+ \frac{Et}{2} \int_0^L\!\!\int_0^{2\pi R} \left\{ \left(\nabla^2 \phi\right)^2 + 2(1+\nu)\left[(\phi_{xy})^2 - \phi_{xx}\phi_{yy}\right] \right\} \mathrm{d}y\mathrm{d}x \\ &- \tau t \int_0^L\!\!\int_0^{2\pi R} w_x w_y \,\mathrm{d}y\mathrm{d}x - Et \int_0^L\!\!\int_0^{2\pi R} \phi \left[\nabla^4\phi + \rho w_{xx} - (w_{xy})^2 + w_{xx}w_{yy}\right] \mathrm{d}y\mathrm{d}x. \end{aligned} \tag{1}$$

where $w(x, y)$ is the radial deflection and $\phi(x, y)$ is a stress function. The first term is the bending energy, the second is the membrane energy, the third is the work done by the externally applied torque $T = 2\pi R^2 \tau t$, and the fourth is an extra energy term resulting from the constraint condition familiar from the von Kármán–Donnell equations, linking the stress

function ϕ to the change in Gaussian curvature of the w-surface. In a Rayleigh-Ritz or Galerkin formulation, modeshapes,

$$\begin{aligned} w(x,y) &= A_1 \sin^m\left(\frac{\pi x}{L}\right) \sin\left(\frac{\lambda x}{L} - \frac{ny}{R}\right) + A_2 \sin^2\left(\frac{\pi x}{L}\right), \\ \phi(x,y) &= B_1 \sin^m\left(\frac{\pi x}{L}\right) \sin\left(\frac{\lambda x}{L} - \frac{ny}{R}\right) + B_2 \sin^2\left(\frac{\pi x}{L}\right), \end{aligned} \tag{2}$$

are assumed, where A_i and B_i are unknown amplitudes. The power $m = 1, 2$ accommodates both simply-supported and clamped boundary conditions at the ends of the twisted length. Linear eigenvalue analysis for the critical torque T^C sets A_2 and B_2 to zero and minimises with respect to A_1, B_1, n and λ. Comparisons with experiments are given in Table 1.

Table 1. Comparisons between experiments of Yamaki [1], and linear eigenvalue results for which $\gamma = \arctan(nL/\lambda R)$.

	length L [mm]	22.9	35.9	51.0	71.2	113.8	160.8
Experiment	crit. torque T^C [Nm]	99	64	51	41	33	28
	w/number n	23	21	19	17	15	13
	obliqueness γ [deg.]	44	56	59	67	73 or 69	70
Simple	T^C [Nm]	93.2	62.2	48.1	38.8	29.4	24.3
Supports	n	22	20	18	16	13	11
$(m = 1)$	γ [deg.]	59	63	67	70	75	77
Clamped	T^C [Nm]	115.7	71.3	53.6	42.6	32.0	26.3
Supports	n	23	21	19	17	14	12
$(m = 2)$	γ [deg.]	56	61	65	69	73	76

FIRST-ORDER POST-BUCKLING ANALYSIS

If the full waveshape of equation (2) is adopted, A_1 and B_1 interact with A_2 and B_2 in a symmetry-breaking manner such that inwards deflection can be greater than outwards, as seen in Figs.1 and 2. Results of such a post-buckling analysis for a typical paper specimen are given in Table 2. Minimization is carried out at each stage with respect to the obliqueness

Table 2. Change of orientation γ in the post-buckling range ($R = 21.5$ mm, $L = 19$ mm, $t = 0.106$ mm, $n = 9$).

A_1	0.0	0.1	0.2	0.3	0.4	0.5	0.6	0.7
T/T^C	1.000	0.945	0.791	0.573	0.360	0.216	0.135	0.087
γ[deg.]	53.3	53.7	54.4	55.3	55.2	53.1	49.7	46.4

measure, γ. The reduction in γ as the post-buckling develops shows that the crest and valley lines become more oblique as the system adjusts to accommodate the folding mechanism. This same rotation of fold and valley lines is apparent in the comparisons of Table 1, where the experimental values of γ are always less than those for the linear eigenvalue problem applicable at the first stage of buckling only. To accommodate the mechanism fully, crest and valley lines should rotate by different amounts, although this facility is not available within the limitations of the Rayleigh-Ritz approximation.

TRUSS ANALYSIS

For the apex of each elemental triangle of Fig.1 to fold to a point on the circumference, geometry dictates that $\alpha = \pi/n$. A simple triangulated truss formulation based on this constraint (see Fig.3) shows that, after the initial instability, the applied torque decreases rapidly to almost zero in the final folded state. Comparative results will be presented at the time of the conference.

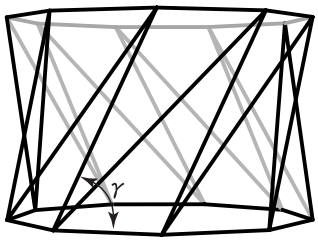

Figure 3. Truss model related to geometry of Table 2 ($R = 21.5$ mm, $L = 19$ mm, $n = 9$).

References

[1] Yamaki, N. 1976. Experiments on the post-buckling behaviour of circular cylindrical shells under torsion. *In:* Budiansky, B. (ed), *Buckling of Structures, IUTAM Symposium, June 1974, Cambridge, USA.* Applied Mathematics and Mechanics. Springer-Verlag.